



## CONVENTIONAL CONSTRUCTION STEEL BRACES WITH BEARING PLATE ENERGY DISSIPATION

C. Wang<sup>(1)</sup>, A. González Ureña<sup>(2)</sup>, M. Afifi<sup>(3)</sup>, A. Rudman<sup>(4)</sup>, R. Tremblay<sup>(5)</sup>, C. A. Rogers<sup>(6)</sup>

<sup>(1)</sup> Ph.D. candidate, Dept. of Civil Engineering and Applied Mechanics, McGill University, chen.wang5@mail.mcgill.ca

<sup>(2)</sup> Ph.D. candidate, Dept. of Civil Engineering and Applied Mechanics, McGill University, andres.gonzalezurena@mail.mcgill.ca

<sup>(3)</sup> Ph.D. candidate, Dept. of Civil Engineering and Applied Mechanics, McGill University, mohamed.afifi@mail.mcgill.ca

<sup>(4)</sup> MEng Thesis candidate, Dept. of Civil Engineering and Applied Mechanics, McGill University, alina.rudman@mail.mcgill.ca

<sup>(5)</sup> Professor, Dept. of Civil, Geological and Mining Engineering, Polytechnique Montréal, robert.tremblay@polymtl.ca

<sup>(6)</sup> Professor, Dept. of Civil Engineering and Applied Mechanics, McGill University, colin.rogers@mcgill.ca

### Abstract

The principle of capacity-based design is used extensively in the seismic design of steel structures. It relies on the inelastic ductility of the Seismic Force Resisting System (SFRS) to dissipate seismic energy. However, in Canada there exists the Conventional Construction (CC) category of lateral frame, for which the engineer is allowed to waive the capacity-based design principles and design a SFRS which is expected to behave principally elastically when subjected to design-level earthquakes. Type CC concentrically braced frame systems do not depend on tensile yielding of the braces to dissipate earthquake energy. Instead, the energy dissipation in tension is expected to mainly occur through localized yielding of connection components and friction within these joints. For structures located in moderate and high seismic regions, if one cannot prove that the brace connections will perform in such a ductile fashion during an earthquake, a 1.5 penalty is applied to the connection design forces as per the CSA S16 Steel Design Standard. Given that there does not exist a codified method to predict the ductility or probable resistance and failure mode of each connection type, practicing engineers most often incorporate this force penalty in design. Although Type CC concentrically braced frames are used extensively throughout Canada, there is limited research available to give insight on the ductility of these systems, particularly in the case of I-shaped braces with bolted end connections.

To address this issue, a study was initiated which comprised the testing and numerical modelling of Type CC braces modified with bolted connections detailed to develop ductile bearing response. The objective of this research was to measure the response of these full-scale I-shape braces and their modified bolted connections under reversed cyclic seismic loading. A design approach for the test specimens was taken in which the probable resistances of the various failure modes of the brace connections were estimated. This information was used to design the flange bolt connections with welded steel bearing plate elements specially detailed to permit inelastic bolt bearing deformations to take place prior to all other failure modes. Two common connection configurations for I-shape braces were studied: a flange plate connection and a flange angle connection, both attached to the gusset plate. These connections were modified to include weld attached bearing plates on the flange plates and angles; the bearing plates rely on the plastic bearing deformations at the bolt holes to develop ductility and dissipate energy. The intent is to improve the predictability in the ductility and resistance of the connections such that the 1.5 force penalty can be eliminated in design. The paper includes a summary of the laboratory test program and the complementary finite element models, with commentary on the implemented design approach and on the ability of these Type CC braces modified with special bearing plates to exhibit ductile behaviour.

*Keywords: steel braced frames; braces; bearing plates; connections*



## 1. Introduction

The design of steel structures for seismic loading typically requires the implementation of capacity design principles, which in terms of energy dissipation engage the inelastic ductility of selected members of the Seismic Force Resisting System (SFRS). In many steel design standards, the seismic energy of concentrically braced frames (CBFs) is dissipated through yielding of bracing members; the other structural components in the lateral load path are designed for the probable capacity of the braces in tension and compression. However, there also exists in Canada the Conventional Construction (CC) category of CBF, as described in the National Building Code of Canada (NBCC) [1] and as outlined in the CSA S16 Standard [2], for which the engineer may ignore capacity design principles and design a SFRS which is expected to behave principally elastically when subjected to design-level earthquakes. These Type CC systems are designed using low seismic force modification R-values ( $R_o = 1.3$  &  $R_d = 1.5$ ) [1], and hence do not depend on extensive yielding of selected members to dissipate earthquake energy. As an alternative, energy dissipation is assumed to occur through limited yielding in members and connections along the lateral load path, as well as through friction within the joints. In moderate and high seismic zones, the CSA S16 Standard requires the seismic forces for the connections in the lateral load path of Type CC systems be increased by a factor of 1.5, if it cannot be proven that these connections have an expected failure mode that is ductile. However, no guidelines or recommendations are given in codified format to determine the ductility of connections. As such, most connections for Type CC systems are designed with seismic loads that are effectively elastic, that is, with  $R_o R_d = 1.3$ .

Rudman et al. [3] measured the response of six full-scale Type CC I-shape braces and their bolted connections under reversed-cyclic seismic loading. The test program comprised two I-shape section sizes (W310×97 & W360×134 ASTM A992 Gr. 50), and two commonly used bolted connection types: one with plates transferring the load from the I-shape to the gusset plate and the other using angles for this purpose. In the design of these specimens, a capacity-based approach was not implemented and no hierarchy was placed on desirable failure modes. A thorough description of the design method and prior test program is available in the thesis of Rudman [4]. To supplement these initial test specimens, two additional brace specimens were designed and tested in a similar fashion. However, in this case, a decision was made to target the bolt bearing failure mode in special plates incorporated in the brace connection as the desirable means of dissipating energy in this otherwise Type CC system. A design approach, beyond what is presently found in the CSA S16 Standard, was used in which both the factored and probable bearing resistances of the bearing plates were set to be lower than all other factored and probable failure modes, respectively, including shear fracture of the bolts. A description of this supplementary test program and the subsequent finite element modelling is provided herein, with commentary as to the effectiveness of this attempted method to improve the ductility of Type CC brace connections.

## 2. Laboratory test program

### 2.1 Design of test specimens

The two test specimens, designated as Specimen J360-P & C360-P, were of the same brace size W360×134 and grade ASTM A992 Gr. 50 as that used by Rudman et al. [3]. The factored design buckling capacity of the braces was determined to be 3680 kN, assuming a buckling length of 6 m (using a corner-to-corner length of 6.67 m multiplied by a K factor of 0.9). The connecting components were designed such that the limiting factored tensile resistance, as calculated using the resistance equations from the CSA S16 Standard [2], was greater than the factored design buckling load of the brace. The 1.5 factor for non-ductile connections in Type CC-type braces, as prescribed in CSA S16 Clause 27.11.1 [2], was not used in these calculations. Specimen J360-P comprised a flange plate connection at brace ends, whereas Specimen C360-P was constructed using angles to transfer flange forces to the gusset plates. In comparison to the initial six specimens tested by Rudman [4], bearing plates were welded to the flange plates of Specimen J360-P and the



angles of Specimen C360-P, as shown in Figure 1. The webs of both specimens were attached with plates on both sides and bolts in double shear, in the same fashion as for the first six specimens by Rudman.

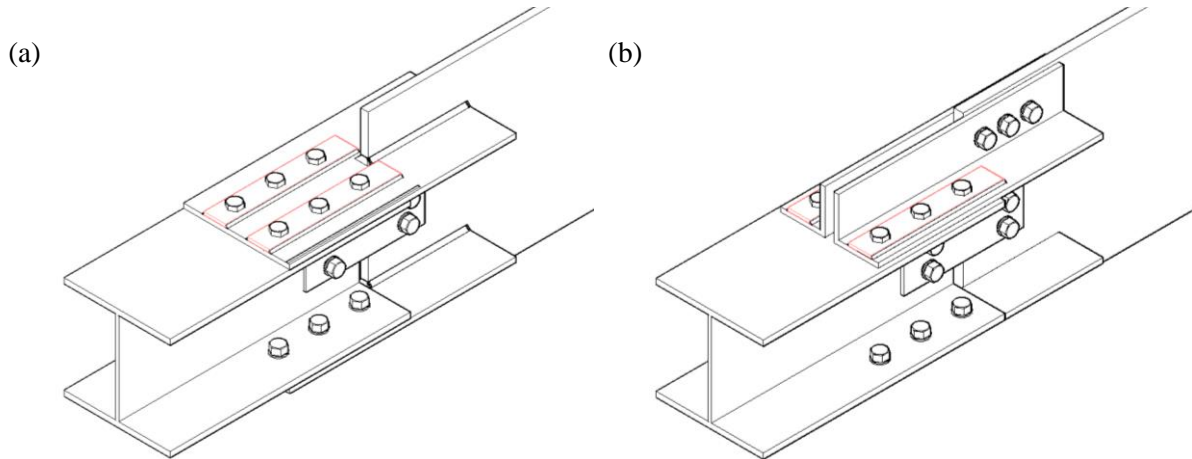


Fig. 1 – Modified bolted I-shape brace connections with bearing plates: (a) modified flange plate connection J360-P, (b) modified flange angle connection C360-P

The connections were modified from the original six specimens in an attempt to improve the overall ductility. This was done by designing a thinner sacrificial plate to have a low bearing capacity, allowing the flange bolts to bear onto this plate before attaining any other ultimate failure mechanism. As a result, the bearing plates would become a fuse during a significant seismic event. To achieve a decreased bearing capacity, large diameter bolts (1-1/8" (28.6 mm) ASTM F3125 A490) were chosen so that fewer fasteners could be used compared with the test specimens of Rudman et al. [3]. The connecting flange plates and angles, to which the bearing plates were welded, had slotted holes (2-13/16" (71.4 mm) in length) to allow the bolts to bear onto the bearing plates, which had standard hole sizes (1-3/16" (30.2 mm)), for a predetermined bearing distance based on estimates of deformation demands [4]. A close-up of this bolt hole design is shown in Figure 2a. The bearing plates, 9.5 mm × 76 mm wide (ASTM A572 Gr. 50) were attached to the connecting plates or angles using 6 mm fillet welds on both longitudinal sides (Fig. 2b,c).

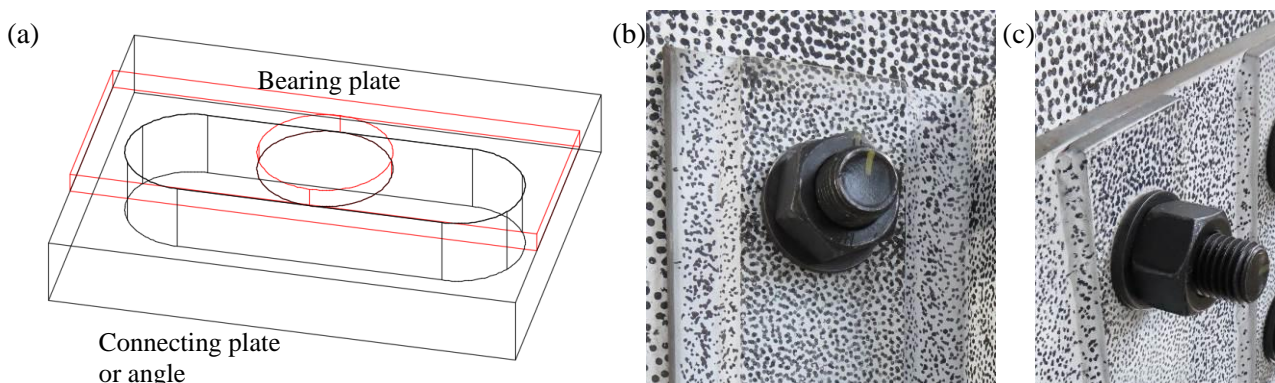


Fig. 2 – Close-up view of fuse-type bearing plate connection: (a) schematic drawing, (b) flange angle connection C360-P, (c) flange plate connection J360-P



The factored bearing resistance of the plates was determined with CSA S16 [2] as 3527 kN, which is similar to the factored buckling capacity of the braces. The bolt shear fracture failure mode was the next highest resistance with a predicted capacity of 3825 kN (threads not in the shear plane). All other anticipated failure modes were calculated to have factored resistance values greater than that of the plates in bearing (see Rudman [4]). According to CSA S16, this would indicate that the bearing failure mode should occur prior to shear fracture of the bolts. To further confirm this hierarchy of failure modes, the probable resistances of the plates in bearing and the bolts in shear, along with other anticipated failure modes, were determined by setting the resistance factor,  $\phi$ , equal to 1.0 and applying an estimated overstrength; a value of 1.1 was used for both the bolt bearing and bolt shear failure modes. Note, this approach to capacity to design is not explicitly provided in the CSA S16 Standard. This resulted in probable resistances of 4850 kN for bolt bearing on the plates and 5254 kN for shear fracture of the bolts; the other probable resistances exceeded these values. As such, the design calculations indicated that failure in the test specimens would comprise bearing deformations of the supplemental plates that were welded to the connecting flange plates (Specimen J360-P) and angles (Specimen C360-P).

Table 1 – Summary of brace and connection test specimen components

Design Element	Parameter	J360-P	C360-P
Brace	Size	W360×134	W360×134
Bolts	Grade	A490	A490
	Size (mm/in)	28.6 (1-1/8")	28.6 (1-1/8")
	No. rows per flange	3 rows × 2 bolts	3 rows × 2 bolts
	No. rows in web	1 row × 2 bolts	1 row × 2 bolts
Bolt spacing	End distance in flanges (mm)	59	59
	Spacing in flanges (mm)	121	121
	Gauge in flanges (mm)	152	210
	End distance in web (mm)	117	117
	Gauge in web (mm)	79	79
Angles	Section	NA	L152×152×16
	End distance (mm)	NA	59
	Spacing (mm)	NA	121
	Gauge to heel (mm)	NA	89
Web plates	Width (mm)	175	175
	Thickness (mm)	9.5	9.5
Flange plates	Width (mm)	368	NA
	Thickness (mm)	15.9	NA
	Welds D (mm) / Length (mm)	11 / 4 × 343	NA
Gusset plates	Thickness (mm)	25	32
Bearing plates	Width (mm)	76	76
	Thickness (mm)	9.5	9.5
	Welds D (mm) / Length (mm)	6 / 2 × 457	6 / 2 × 457

The I-shape braces in this project were fabricated with ASTM A992 Gr. 50 steel, the plates were fabricated with ASTM A572 Gr. 50 steel, and the angles were fabricated with ASTM A6 Gr. 44 steel. The nominal yield stress ( $F_y$ ) for the braces and the plates was 345 MPa, while the nominal tensile stress ( $F_u$ ) was



450 MPa. For the angles, the nominal  $F_y$  was 300 MPa and the nominal  $F_u$  was 450 MPa. The ASTM F3125 A490 bolts have a nominal  $F_u$  of 1035 MPa. An E71T (nominal  $F_u = 490$  MPa) electrode was used in a flux-cored arc welding process with additional shielding gas ( $\text{CO}_2$ ) for all fillet welds. A listing of the components for each test specimen is provided in Table 1.

## 2.2 Test setup, instrumentation and loading protocol

The two specimens were tested in a 12 MN MTS load frame in the Structural Engineering Laboratory at Polytechnique de Montréal. The specimens were assembled in the frame with a specially designed grip at each end, as shown in Figure 3. The grips were clamped on the T-stub ends of the gusset plates and were then bolted to the strong floor and the actuator piston's platen. The grips were designed to simulate the restraint conditions on a gusset plate when it is welded to a beam-column joint in a building structure. The specimens were designed to be 6.67 m in length between the ends of the gusset plates.

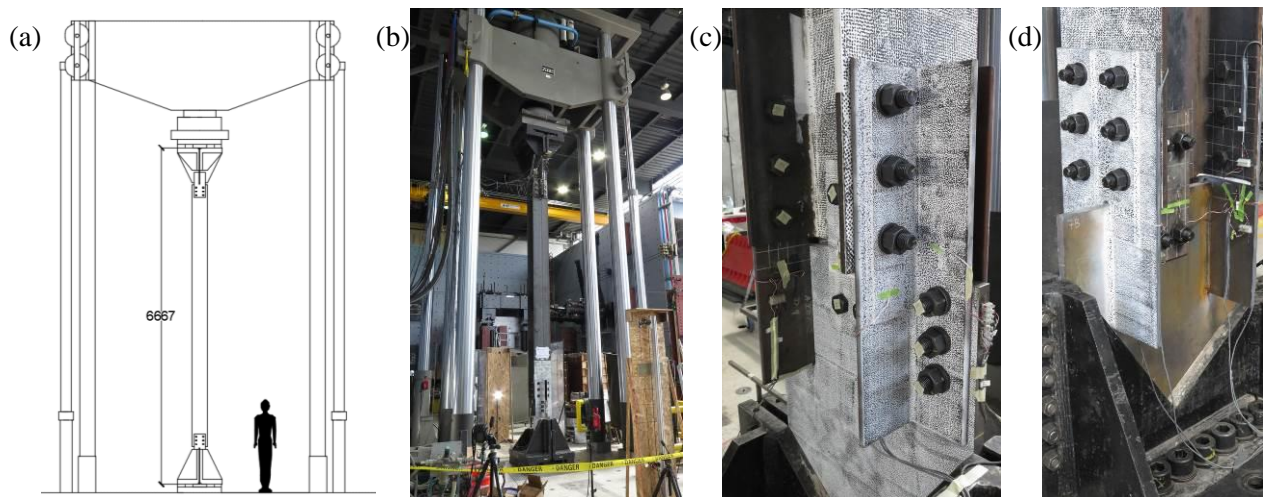


Fig. 3 – Brace test assembly in 12 MN universal testing machine: (a) schematic drawing, (b) full setup, (c) base flange angle connection (Specimen C360-P), (d) base flange plate connection (Specimen J360-P)

Photographs of the overall test setup (Fig. 3b), Specimen C360-P with the flange angle connection (Fig. 3c) and Specimen J360-P with the flange plate connection (Fig. 3d) have been provided. The bearing plates can also be seen in Figures 3c and 3d. Pretensioning of the bolts was done during installation using the turn-of-the nut method.

The 12 MN MTS load frame captured displacement data with an internal LVDT and load data via a load cell. MTS Series 793 software was used to control the actuator, while the MTS TestSuite Multipurpose Elite software was used to implement the loading protocol. In addition, three types of instrumentation were used to collect data during testing: string potentiometers and linear potentiometers for axial and out-of-plane displacements, strain gauges for local strains, and a digital image correlation (DIC) systems for the base connection. The measurement instruments (except the DIC system) were connected to Vishay Model 6100 scanners that were used to record data at ten scans per second using the Vishay System 6000 StrainSmart software. At the base of each brace test specimen, three DIC camera systems (Correlated Solutions Inc.) were used to capture the movements of a speckle pattern that was painted onto the visible portion of the gusset plate, the connecting plates, and the base of the brace on the North, South, and East sides (Fig. 3c,d). Each DIC camera system consisted of two Sony ICX625 cameras (type CCD 2/3" 5MP FireWire): one camera positioned at an angle above the connection and the other positioned at an angle below the connection. The VIC-Snap version 8 software was used for the image capture. These images were then processed in VIC3D version 8 to extract the displacements and strains.



The loading protocol was consistent with that developed by Rudman [4] for the previous six Type CC brace test specimens [3]. It was developed using information obtained from a pre-testing numerical study, in which five Type CC CBF structures were designed for Vancouver and Montreal Canada on soil classes E and C. Nonlinear dynamic analysis of the model buildings was carried out using a suite of scaled ground motions. The deformation demands in the brace connections were obtained, and the displacement response histories of the connections were used to create a representative reversed-cyclic loading protocol. The initial six cycles were run in force control (60 kN/s) with load targets set at 30% of the expected buckling load, to ensure that the specimen remained in the elastic range. All remaining cycles were applied in displacement control at a rate of 0.5 mm/s. The opening loading direction for each cycle was in compression. In the laboratory study by Rudman et al. [3] the initial large tension excursion of the first specimen that was tested came close to the anticipated failure resistance of the specimen. As such, it was decided that the approximate length of the measured slip plateau (7 mm) [4], plus the average yield displacement found in Castonguay's [5] connection tests (8.2 mm), would serve as the  $\delta_y$  of 15.2 mm in the loading protocol for the remaining cycles and the following specimens. A detailed description of the loading protocol (Fig. 4) and its development is provided by Rudman [4].

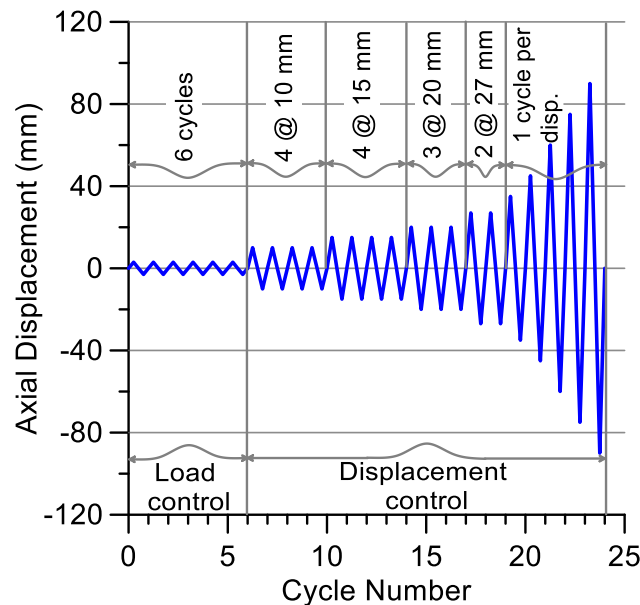


Fig. 4 – Representative loading protocol for Specimens J360-P and C360-P

### 2.3 Test results

A photographic summary of the damage patterns observed for the flange plate brace connection test specimen (J360-P) is provided in Figure 5, while similar information is shown in Figure 6 for the flange angle brace connection test specimen (C360-P). The axial load vs. overall displacement (storey drift) for each test specimen is shown in Figure 7.

The J360-P flange plate connection specimen exhibited inelastic deformations in the connections during tension cycles. The brace underwent overall minor axis buckling (Fig. 5d) during compression cycles, while the gusset plates also rotated out-of-plane. During the tension cycles, the brace would straighten and extensive inelastic deformations were observed in the web of the I-shape (block shear Fig. 5c), and bearing deformations occurred in the four bearing plates (Fig. 5a) at the base of the test specimen. At ultimate load, the bolts connecting the flanges to the flange plates at the base of the test specimen failed in a combined shear and tension mode (Fig. 5b). Noticeable deformations of these fasteners at both the top and base of the brace occurred prior to their fracture. The observed failure mode at ultimate did not coincide with the predicted mode as identified using the probable resistance values. Although the flange bearing plates did exhibit extensive



bearing deformation, the limiting force achieved by the test specimen was a result of the sudden fracture of the bolts on a tension cycle. Note, a single flange bolt broke in the penultimate tension cycle. In the subsequent and final tension cycle, the remaining 11 flange bolts broke at the base of the test specimen in a sudden and rapid manner.

The C360-P flange angle connection specimen also exhibited inelastic deformations in the connections during tension cycles. The brace underwent overall minor axis buckling during compression cycles which was accommodated by the out-of-plane rotation of the gusset plates. As the brace straightened during the tension cycles extensive inelastic deformations were observed in the web of the I-shape (block shear Fig. 6c), and bearing deformations occurred in the four bearing plates attached to the angles (Fig. 6a) at the base of the test specimen. At ultimate load, the upper bolts connecting the flanges to the flange angles on the west side at the base of the test specimen failed in a combined shear and tension mode (Fig. 6a,b). The sudden loss of load transfer on this side of the brace caused an eccentric loading of the bolts on the east side of the brace, with those connecting the gusset plate to the angles then fracturing. This was likely due to the additional force placed on these bolts resulting from the eccentric axial force in the I-shape brace considering that in the last stages of testing only a single flange was attached. Deformations of the fasteners at both the top and base of the brace occurred prior to their fracture. Again, the observed failure mode at ultimate did not coincide with the predicted mode as identified using the probable resistance values. The bearing plates welded to the connecting angles did exhibit bearing deformation, however, the test specimen's maximum force was bounded by the sudden fracture of the bolts on one flange during a tension cycle.

The axial load vs. overall displacement (storey drift) graph for test specimen J360-P (Fig. 7a) illustrates that the overall buckling capacity of the brace was attained (5392 kN), followed by a significant reduction in compression resistance in the post-buckling range. During the tension cycles, a plateau was reached repeatedly due to the capped bearing resistance of the bearing plates. However, after recurring cycles this bearing resistance increased due to the accumulated deformations in the plates, which then led to the fracture of the bolts at 5761 kN, and the complete loss of load carrying ability. Bolt slip was also evident whenever the direction of loading was reversed; this did provide for additional energy dissipation in the connections at both ends of the brace prior to fracture of the bolts. An equivalent storey drift of approximately 2.37% was reached for the tension cycles prior to fracture of the bolts. The overall buckling of the brace was observed to occur at 0.97% equivalent storey drift during the compression cycles.

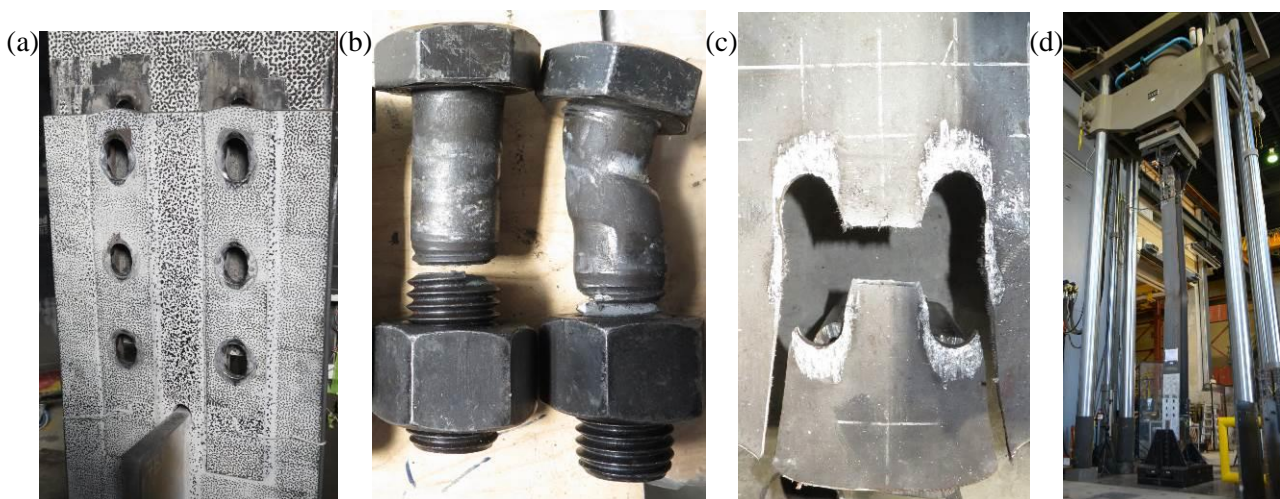


Fig. 5 – Observed damage in flange plate connection (Specimen J360-P): (a) bearing deformations in fuse plates, (b) bolt fracture, (c) block shear failure in web of brace, (d) overall buckling of brace



Similarly, the axial load vs. overall displacement (storey drift) graph for test specimen C360-P (Fig. 7b) provides information as to the failure modes and response of the brace and its connections. The overall buckling capacity of the brace (5418 kN) was reached at 1.67% equivalent storey drift. The compression resistance then quickly decreased. No additional compression cycles were applied to the test specimen after this buckling, because of the subsequent tension cycle failure of the bolts, as described above, at a force level of 5131 kN. During the tension cycles the bearing deformations of the bearing plates were not as extensive as seen for specimen J360-P; rather, at an equivalent storey drift of 1.44% the bolts fractured, thus limiting the development of a bearing plateau. Once again, bolt slip occurred as the direction of loading was reversed; this did provide for additional energy dissipation in the connections at both ends of the brace prior to fracture of the bolts.



Fig. 6 – Observed damage in flange angle connection (Specimen C360-P): (a) bearing deformations in fuse plate and bolt fracture, (b) bolt fracture, (c) block shear failure in web of brace

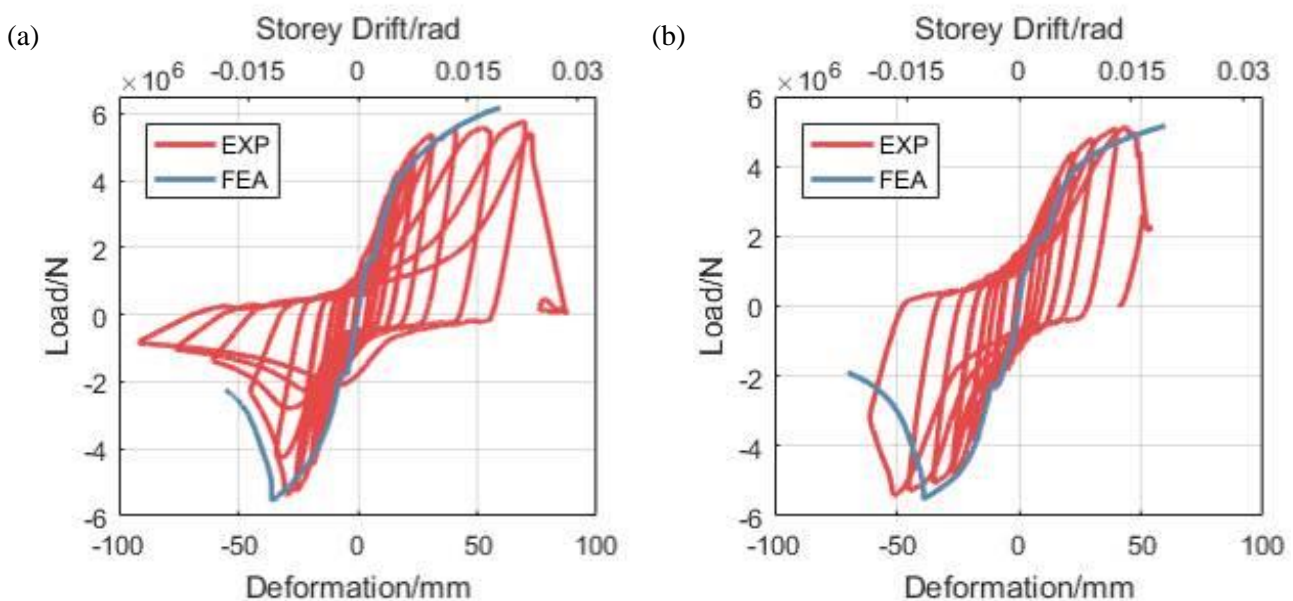


Fig. 7 – Axial load vs. overall displacement (storey drift): (a) Specimen J360-P brace with flange plate connection, (b) Specimen C360-P brace with flange angle connection



Even though the bolts at the base of both specimens did fail in shear, overall inelastic deformations of the braces and their connections were observed. However, considering that capacity protection procedures were implemented in the design of the bearing plates for both specimens, the extent of these inelastic deformations was not markedly better than that measured for the six Type CC brace specimens by Rudman et al. [3], for which no capacity protection had been included in design. The comparable test specimens composed of the same brace size and connection configuration, without the bearing plates, reached a similar axial displacement (equivalent drift ratio) in comparison with the two specimens described herein. It appears that the attempt to improve the ductility of the Type CC brace using the bolt bearing deformation mode as a fuse type element was not as successful as originally thought prior to testing, largely due to the difficulty in predicting the probable capacity of the plates as bolt bearing deformation accumulated with repeated loading cycles. In the case of test specimens J360-P and C360-P, the shear resistance was sufficiently close to the predicted bearing resistance, an 8% margin based on probable predictions, that only a small increase in the bearing capacity of the actual brace connection, coupled with fasteners subjected to both shear and tension due to the gap between the brace flange and bearing plates, led to an undesirable failure, sudden bolt rupture in this instance.

Coupons were fabricated from all components of the test specimens and tested according to ASTM A370. The measured material properties are available in Table 2.

Table 2 – Measured material properties of test specimen components

Component	$F_y$ (MPa)	$F_u$ (MPa)
J360-P		
W360×134 Flange / Web	371 / 415	480 / 509
Flange plate	415	505
Web plate	420	502
Bearing plate	420	502
Gusset plate	382	531
C360-P		
W360×134 Flange / Web	360 / 377	480 / 487
Angle	399	534
Web plate	420	502
Bearing plate	420	502
Gusset plate	402	590

### 3. Finite element modelling

Numerical simulation based on 3D continuum finite element (FE) analysis was conducted to better understand the behaviour of the tested specimens using Abaqus 6.14 [6]. The elements of type C3D8R (3D 8-node brick elements with reduction) were used, and refined meshes were adopted in areas of potentially high plasticity, e.g. bolts and plates in the vicinity of bolt holes. A linear kinematic hardening model was used to describe the steel strain hardening; the material property parameters were determined based on the steel tension coupon test results from Rudman [4]. Due to the formidable size of the model, and the large number of contacts, which are quite computationally demanding, only monotonic loading was simulated in separate runs for the tension and compression directions.

The force-deformation curves obtained through the FE modeling were also plotted in Figure 7; these matched well with the back-bone curves of the measured laboratory response. Both simulations accurately predicted the buckling modes (minor axis brace buckling) and the buckling resistances. The tension loading



simulation captured comparable deformation to the tests, with typical plate bearing and web block shear modes shown in Figure 8, along with the bolt deformations illustrated in Figure 9.

Both laboratory test specimens failed by rupture of the bolts connecting the brace flanges and bearing plates. A verification of the bolt behaviour through FE simulation revealed that due to the 15.9 mm gap between the bearing plates and the brace flanges (slot in the flange plate for J360-P and slot in the flange angle for C360-P (Fig. 2a)), the bolts connecting them were subjected to both shear and bending, instead of the assumed single-plane shear as was used in their design. In addition, significant tensile forces were applied to the bolts due to the inclined position caused by the single shear force transfer mechanism from the brace flange to the flange plates or angles in tandem with the gap between these plates. A typical stress distribution of the bolt is shown in Figure 9, along with details of the slotted connection through to the bearing plate. The noticeable existence of both bending and tension, caused by the combined gap between the bearing plate and I-shape brace flange, along with the single shear loading scenario, is believed to have deteriorated the bolt shear resistance.

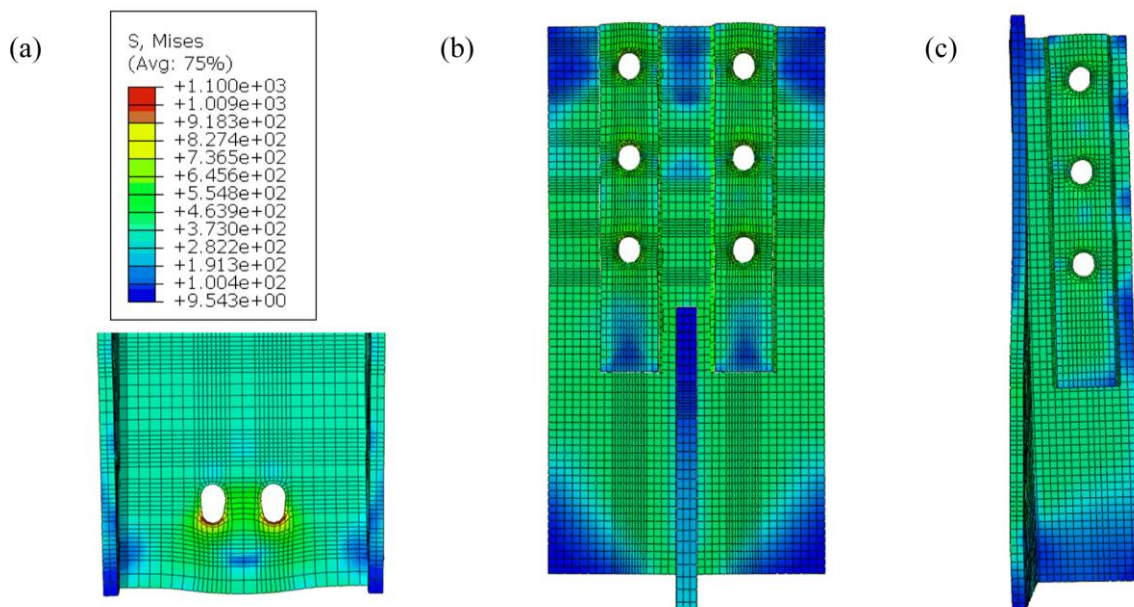


Fig. 8 – Typical deformation in simulation: (a) bearing of brace web in Specimen J360-P; (b) deformation of bearing plates in Specimen J360-P; (c) deformation of bearing plates in Specimen C360-P

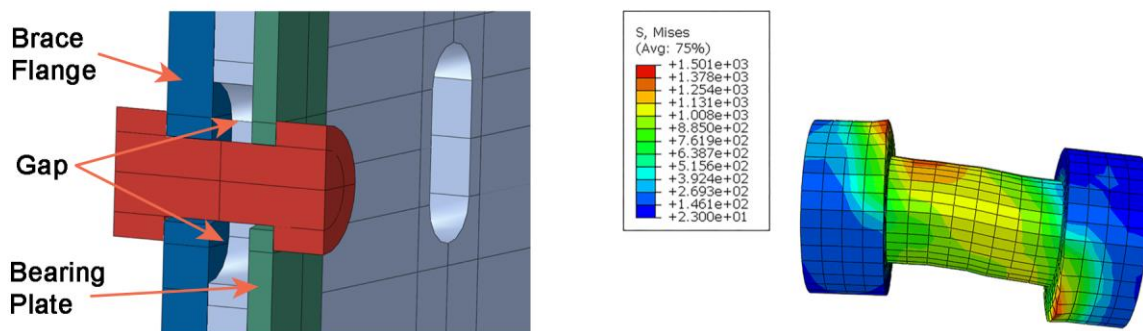


Fig. 9 – Stress distribution of a bolt connecting bearing plates and brace flanges in Specimen J360-P



As used in the design of the test specimens, the factored bearing resistance of the bearing plates, and the factored shear resistance of bolts in the flange plates, 3527 kN and 3825 kN, respectively, according to CSA S16 [2], indicated that the bearing failure mode would occur prior to shear fracture of the bolts. Similarly, if probable resistances were determined in design by setting the resistance factor,  $\phi$ , equal to 1.0 and applying an overstrength of 1.1 for both failure modes, the bearing of the plates, 4850 kN, remained lower than the shear fracture of the bolts, 5254 kN. In contrast, the FE modelling demonstrated that the bearing forces could reach higher values than that predicted in the design phase of the research. Furthermore, the force developed by all bearing plates in Specimen J360-P was extracted through numerical simulation and found to be 5200 kN, at the onset of bolt failure. As such, the bearing forces exceeded the obtained pre-test estimate, likely due to the conservative nature of the general formulation in the CSA S16 Standard. The factored resistances calculated based on formulas in CSA S16 do not imply failure hierarchy due to many factors, e.g. inaccuracy of formulas, material variability, overstrength, etc. The attempt at a simple determination of the probable bearing resistance did not provide for an improved prediction of the failure mode of these test specimens. Hence, the FE models confirm the response observed during testing. Although some bearing deformations occurred in the dedicated bearing plates, the forces necessary to cause these deformations reached a level that triggered shear fracture of the flange bolts, a failure situation that was not anticipated based on the CSA S16 factored and probable design calculations.

#### 4. Conclusions

A study on the performance of Type CC braces and connections was carried out, whereby bearing plates were introduced in the connection in an attempt to control and improve the ductility offered during a design level seismic event. The study comprised a laboratory phase and a numerical phase, which combined were used to identify the resulting performance of these I-shape braces and their connections. Two I-shape section sizes (W310×97 & W360×134), and two commonly used bolted connection types (flange plate & flange angle) were included in both the laboratory and numerical studies.

Considering that capacity protection procedures were implemented in the design of the bearing plates for both specimens, the extent of the inelastic deformations of the braces and their connections under tension loading was not markedly better than that measured for the six Type CC brace specimens previously tested by Rudman et al. [3], for which no capacity protection had been included in design. The attempt to improve the ductility of the Type CC brace using the bolt bearing deformation mode as a fuse type element was not as successful as originally thought prior to testing. This occurred due to the difficulty in predicting the probable bearing capacity of the plates as the bolt bearing deformation accumulated with repeated loading cycles. The bolts' shear resistance for the two specimens was sufficiently close to the predicted bearing resistance, that only a small increase in the bearing capacity of the actual brace connection, coupled with fasteners subjected to shear, flexure and tension due to the 15.9 mm gap (thickness of flange plate J360-P & thickness of flange angle C360-P) between the brace flange and bearing plates, led to an undesirable failure, sudden bolt rupture in this instance. If bolt bearing is to be defined as a means to obtain a more ductile connection response to seismic loading it is recommended that the margin between the probable bearing resistance and that of any other failure modes, especially bolt shear rupture, be such that a repeat of the performance observed in this study does not occur.

#### 5. Acknowledgements

The authors would like to thank DPHV Structural Consultants, and ADF Group Inc. for their generous technical and financial support, as well as the Natural Sciences and Engineering Research Council of Canada (NSERC), the Fonds de Recherche du Québec – Nature et Technologies (FRQ-NT) and the Centre d'Études Interuniversitaire des Structures sous Charges Extrêmes (CEISCE). The finite element computations were conducted on the supercomputer Graham cluster, which is managed by Calcul Québec and Compute Canada. The supercomputer operation is funded by the Canada Foundation for Innovation (CFI), NanoQuébec, RMGA and the Fonds de recherche du Québec - Nature et technologies (FRQ-NT). The authors also express



their appreciation to the technical staff of the Structural Engineering Laboratory at Polytechnique Montréal and undergraduate research assistants Mairvat Abdulhamid and Jacob Burke.

## 6. References

- [1] NRCC (2015): National building code of Canada, 14<sup>th</sup> edition. National Research Council of Canada, Ottawa, ON, Canada.
- [2] CSA (2014): CSA S16-14 Limit state design of steel structures. Canadian Standard Association, Mississauga, ON, Canada.
- [3] Rudman A, Tremblay R, Rogers CA (2019): Seismic performance of Conventional Construction I-shape brace members and their bolted connections undergoing reversed cyclic loading. *12th Canadian Conference on Earthquake Engineering*, Quebec, Canada.
- [4] Rudman, A (2018): Testing of conventional construction W-shape brace members and their bolted end connections undergoing reversed cyclic loading. Master's thesis, Department of Civil Engineering, McGill University, Montreal, QC, Canada.
- [5] Castonguay, PX (2010): Seismic Performance of concentrically braced steel frames of the conventional construction category. Master's thesis, Department of Civil, Geological and Mining Engineering. École Polytechnique de Montréal, Montreal, QC, Canada.
- [6] Dassault Systèmes (2014): *Abaqus 6.14 Documentation*. Providence, RI: Dassault Systèmes.